Contents lists available at ScienceDirect

Progress in Organic Coatings

journal homepage: www.elsevier.com

Photocurable resin/nanocellulose composite coatings for wood protection

Annalisa Cataldi [a], Carola Esposito Corcione [b,*], Mariaenrica Frigione [b], Alessandro Pegoretti [a]

[a] University of Trento, Department of Industrial Engineering and INSTM Research Unit, Via Sommarive 9, 38123 Trento, Italy
[b] University of Salento, Department of Innovation Engineering, Via Monteroni, 73100 Lecce, Italy

ARTICLE INFO

Article history:
Received 26 September 2016
Received in revised form 12 January 2017
Accepted 16 January 2017
Available online xxx

Keywords:
Photocuring
Cellulose nanocrystals
Microcellulose
Composites
Protective coatings
Wood

ABSTRACT

Novel UV-light curable methacrylic-siloxane-cellulose composite coatings for wood protection were prepared, fully characterized and, then, applied on walnut wood samples in order to assess the potential protective performances of the wooden treated substrates, such as hydrophobicity and surface properties. A comparison between nanocellulose and microcellulose filled coatings (5 and 10 wt%) was also performed. Thermal-mechanical analysis highlighted the higher effectiveness of nanocellulose in increasing the glass transition temperature, improving thermal and dimensional stability and stiffness of the neat photoresin with respect to microcellulose. A more pronounced increase of hydrophobicity (contact angle and water capillarity), surface hardness (Shore D and pencil scratch tests) of the neat UV-light cured matrix filled with nanocellulose and applied on wood was, finally, observed in comparison to microcellulose composites.

1. Introduction

Wood is one of the most used and abundant renewable material in the world. It is utilized for a wide of applications, but its main drawback is the high propensity to decay for various degradative processes [1]. The degradation of wood in artworks and buildings is still an open issue. Environmental agents and microbial attacks combined to the water action are the main causes of wood's decay [2]. In fact, the most frequent and dangerous degradation phenomena are correlated to the presence of water, that can act as a medium to convey aggressive agents or alone, causing internal stresses due to pressure and temperature changes. The capillary rising, for instance, is the most widely phenomenon visible on the facades of the buildings, especially those built with porous wood. These materials have, in fact, a very complex structure, that promotes water absorption by capillarity [3]. Furthermore, biological degradation is very frequent for wood substrates and their repair is still an open issue. In fact, some wood types are very sensitive to biological attacks, due to their microstructure and porosity. All these chemical, physical and/or mechanical degradative processes are catalyzed by the water presence and the overall effect is to impair the mechanical properties of wood t[illegible],5].

Thermal or chemical treatments and impregnation modification have revealed good prospective in reducing water absorption and deformation, rising biological resistance and improving weathering performance [6]. In details, linear anhydrides, aldehydes, furfuryl alcohol,1,3-dimethylol-4,5-dihydroxyethyleneurea (DMDHEU), phenolic or melamine resins, could be considered the most efficient treatments to increase the durability of wood substrates [7,8].

Polymers based on acrylic and metacrylic monomers are extensively used for the protection and conservation of wood, too [9]. Acrylic based coatings, however, have shown durability issues for the protection of outdoor buildings for long time [10–12]. Acrylic coatings generally manifest a reduced adhesion on porous substrates and offer a certain drainage of water from the treated surface [8,13–15].

In addition, most common wood protectives, such as nitrocellulose lacquer, polyurethane, unsaturated polyester and amino acid curing [16], are solvent-based coatings containing volatile organic compounds (VOCs). Some products have benzene, toluene, xylene, and substances of great carcinogenicity, which could damage the environment and human health. Environmentally friendly coatings, such as high-solid-content, waterborne, radiation-curable or powder coatings could substitute the solvent-based coatings [17,18]. In addition, the use of UV-curable wood coatings contributed to the growth of environmentally friendly coatings. UV curing has now been recognized as a substitute curing method to thermal one. The photopolymerization reaction allows a fast chain growth curing reaction, by using photon energy from radiation sources. Furthermore, UV-curable coatings possess superior durability, chemical and stain resistance, as well as faster reaction rates and substantial reductions, or complete elimination, of VOCs [19–23]. There is an increasing attention on the use of cellulose-based fillers as renewable reinforcing agents in order to replace the standard synthetic fillers. In this work the cellulose nanocrystals (CNC) were selected as nanoscale filler.

CNCs are isolated through the acid hydrolysis of natural cellulose fibers [24] or from already hydrolyzed cellulose microcrystals (CMC) [25]. In fact, rod-like CNC particles have interesting properties, in

* Corresponding author.
Email address: carola.corcione@unisalento.it (C.E. Corcione)

http://dx.doi.org/10.1016/j.porgcoat.2017.01.019
0300-9440/

terms of biocompatibility, anisotropy, good optical transparency, low thermal expansion coefficient and, especially, high elastic modulus, similar to steel [26,27].

Interestingly, even if cellulose is a hydrophilic polymer it can promote an increment of the barrier properties of polymeric matrices when dispersed at a nanoscale level [13,28]. In fact, cellulose nanocrystals can produce a reduction of the diffusivity of penetrant liquids thanks to an increase of tortuosity provided by their bonding with the polymer chains [29]. Additionally, the chemical affinity between wood and cellulose-based fillers and the promising preliminary results obtained by the photoresin filled with cellulose microcrystals (CMC) [23] have encouraged the investigation of this nanofiller.

Therefore, the purpose of this work is the development, characterization and application of photopolymerizable siloxane-methacrylic-based resin/CNC, specifically intended for the surface and barrier protection of wood substrates. The comparison between micro- and nanocomposites was performed as well. The nano and microstructured UV cured coatings, obtained by the inclusion of both CNC and CMC, are evaluated as protective coatings on wood with improved performances (i.e. surface properties and hydrophobicity).

2. Experimental

2.1. Matrix synthesis and CNC isolation

The basic components and their content into the formulation of the neat photomatrix are listed below:

- Trimethylpropane trimethylacrylate (TMPTMA), provided by Sigma Aldrich (St. Louis, MO, USA) at 85 wt%;
- Trimethoxypropyl silane methacrylate (MEMO), provided by Dow Corning (Midland, MI, USA) at 10 wt%;
- Poly(dimethylsiloxane)-terminated vinyl (VTPDMS), supplied by Sigma Aldrich at 4.97 wt%;
- Alkoxy- silane compound (MPTS), supplied by Sigma Aldrich at 0.03 wt%;
- Bis(2,4,6-trimethylbenzoyl)-phenylphosphineoxide, supplied by Ciba as IRGACURE 819 (1 pph), was used as photoinitiator.

The synthesis procedure, the composition of the photo-resin and chemical formula of all components are reported in previous works [23,30].

Microcellulose (CMC), specific gravity of 1.56g cm^{-3}, a mean molecular weight of 90.000 g/mol, average aspect ratio of 2.4 as purchased from Sigma Aldrich, USA. Aqueous suspensions of cellulose nanocrystals were obtained through the sulfuric acid hydrolysis of microcellulose according to the method described by Bondeson-Oksman and Cranston-Gray [31,32] with minor modifications. The acid hydrolysis was carried out at 45 °C under vigorous stirring for 120 min, using a 64% w/w sulfuric acid solution, a CMC/acid ratio of 10 g/100 ml and a mechanical mixer. A CMC amount of 20 g was processed each time. The reaction was stopped adding 10 folds distilled water. The acid was removed by two centrifuge cycles at 6000 rpm for 15 min each one. The pH of suspension was neutralized through dialysis using cellulose membranes with a cut-off limit of 3.5 kDa. The suspension was then sonicated for 5 min with a Hielscher UP400S device equipped with a cilindrical sonotrode 3 mm in diameter. An average concentration of about 1.4 wt% of CNC in the suspension was determined by TGA analysis in an isothermal test at 120 °C for 20 min under a nitrogen flow of 100 ml min, in order to allow the complete removal of the solvent. at the end of each process. The obtained CNC was stored at a temperature of −4 °C.

Transmission electron microscopy (TEM) observations of CNCs were performed using a Philips® EM 400 T microscope. The samples for TEM analysis were ultrasonicated for 1 min, in order to allow a better dispersion of nanoparticles. A little drop of solution was deposited on a copper mesh grid and the observations were conducted after the complete evaporation of the water.

2.2. Composites preparation

In order to mix the hydrophobic photoresin to CNCs, the aqueous suspensions of nanocellulose were freeze-dried using a 5Pascal freeze dryer model LIO–5 P (Milano Italy) at a minimum condenser temperature of −50 ± 3 °C and a pressure <3 mbar.

Different amounts of freeze-dried CNC (0, 5 and 10 wt%) were mechanically mixed with the photomatrix by means of a homogenizer (Dispermat® FI SIP) for 1 h at 2000 rpm. The composite solutions were sonicated for 5 min using a 14 mm tip and degassed until a complete removal of air bubbles. The liquid solutions were poured in silicon molds with rectangular cavities of size 15 × 5 x 1 mm^3 for DMTA analysis and 50 × 5 × 2 mm^3 for mechanical tests. Samples for hardness tests and static contact angle measurements were poured in circular cavities in order to obtain disks with a thickness of 10 mm.

UV-polymerization of liquid samples poured in silicon molds was carried out for 24 h in a UVB chamber by the exposure to six UVB lamps model UVB 313EL (Q-lab corporation, UK) with a maximum peak of emission at about 315 nm, a maximum power of 480 W and a typical irradiance of 0.68 W/m^2.

Microcomposites were also prepared by using the same CMC particles utilized for the production of CNC at the filler loadings of 0, 5 and 10 wt%.

Before testing, samples were conditioned at a temperature of 23 °C and a relative humidity of 55% in a chamber with a saturated solution of $Mg(NO_3)_2 \cdot 6H_2O$ until the reaching of a constant weight. Nano- and microcomposite samples were identified by the photomatrix, the filler type and its weight concentration (i.e. the samples named photomatrix-CNC-5 indicates the formulation filled with 5 wt% of nanocellulose).

2.3. Characterization of composites

The rheological measurements of the liquid formulations were performed in a strain controlled Rheometer (Ares Rheometric Scientific) with a plate/plate geometry (radius = 12.5 mm) under steady state mode, at room temperature and a shear rate ranging from 0.05 to 100 s^{-1}. In order to check the repeatability of the results, each test was repeated at least three times.

Microstructural observations of cryofractured surfaces of the neat photomatrix and the corresponding CNC composites were carried out by a Zeiss Supra 40 high resolution FESEM microscope with an accelerating voltage of 1.5 kV and a beam aperture of 20 μm.

Differential scanning calorimetry (DSC) measurements were carried out by using a Mettler Toledo ~~TC15~~ calorimeter. A sample average weight of about 10 mg, a nitrogen flow of 150 ml min^{-1} and covered aluminium crucibles were utilized. A heating stage from 0 to 250 °C by a rate of 10 °C/min was analysed. The glass transition temperature (T_g) was evaluated as the inflection point of the thermograms.

The thermal behavior of the photocured composites was evaluated through thermogravimetric analysis (TGA). A Mettler TG50 thermobalance with uncovered alumina crucibles, in a temperature interval between 25 and 700 °C, at a heating rate of 10 °C min^{-1}, and under a nitrogen flow of 150 ml min^{-1} was used. The onset temperature

(i.e., the temperature associated to a mass loss of 10%), the maximum degradation temperature (i.e. the maximum of the mass loss peak) and the residual mass at 700 °C were determined.

Dynamic mechanical thermal analysis (DMTA) were performed with a TA Instruments DMA Q800 device under tensile configuration. At least three rectangular specimens 15 mm long, 5 mm wide and 1 mm thick were tested in order to estimate the storage modulus (E'), loss modulus (E") and loss factor (tanδ) as a function of temperature in a range between −10 °C and 120 °C, at a heating rate of 3 °C min^{-1} and a frequency of 1 Hz.

The coefficients of linear thermal expansion (CLTE) of nano- and microcomposites were determined through the DMTA analysis of rectangular samples (15 × 5 × 1 mm^3) using a TA Instruments DMA Q800 device under tensile configuration in controlled force mode under a zero applied load in a temperature range from 0 to 150 °C at 6 °C/min.

Three-points bending tests according to ASTM D790 standard were carried out by means of an Instron 4502 universal testing machine. At least 5 rectangular specimens (width 5 mm, thickness 2 mm, span length 40 mm) for each sample were tested with a crosshead speed of 1 mm/min and a 1 kN load cell. The flexural modulus (E_f), the maximum tensile stress ($\sigma_{MAX,f}$) and the maximum tensile strain ($\varepsilon_{MAX,f}$) in each specimens were determined.

Hardness Shore D of UV-light cured samples was obtained using a digital durometer Sh D, Gibitre Instruments, according to ASTM D2240. The thickness of each specimen was 10 mm and 5 specimens were tested for each sample.

The scratch hardness values of the samples were obtained with pencil hardness test, according to ASTM D 3633.

Static contact angle measurements were measured on unfilled and filled samples with a First Ten Angstroms FTA1000 Quick Start instrument, equipped with a video-camera, at room temperature by means of the sessile drop technique, according to NORMAL Protocol 33/89. Thirty measurements were done on each sample, averaging the results. The measuring liquid was bi-distilled water (surface tension γ = 72.1 mN/m).

2.4. Application on wood

The photo-polymerizable protective composites were applied on walnut wood elements as protective coatings in order to confirm if the existence of the coating and the introduction of micro- and nanocellulose are able to decrease the water absorption of this kind of wood. The walnut wood is hard, dense, tight-grained and it can be polisheed to a very smooth finish, which make it attractive for various applications.

A fixed amount (i.e. 1 g/25 cm^2) of each liquid formulation (neat resin and resin filled with CNC and CMC) was applied on one of the surface of the walnut wood samples, by brush. All treated samples were photo-cured by exposure to UV light, working in air atmosphere at room temperature, by using a medium pressure Hg UV lamp (UV HG 200 ULTRA), with a radiation intensity on the surface of the sample of 9.60 μWatt/mm^2. Sets of 10 coated and uncoated specimens (20 × 20 × 20 mm^3) of walnut wood were oven dried at 105 ± 2 °C until a constant weight was reached and then placed in a tank, filled with deionized water for 8 days. Water was replaced with fresh one ~~daily~~ during the immersion period. The samples were periodically removed from the tank, shacked to remove residual water, weighed and their dimensions measured. Then, water absorption values at the time t (WAt) were calculated according to the following equation:

$$WAt = 100\frac{(W_t - W_0)}{W_0} \quad (1)$$

where Wt ~~was~~ the weight of the specimen soaked in water for time t (g) and W_0 ~~was~~ the initial weight of a dry specimen (g).

Static contact angle measurements were performed with a First Ten Angstroms FTA1000 Quick Start instrument, equipped with a video-camera.

The assessment of color alteration on untreated and treated wood elements was carried out by means of a Konica Minolta CR-410 in total reflectance and double channel mode, using a Xenonlamp light source.

Hardness Shore D of the treated and untreated samples was measured using a digital durometer Sh D, Gibitre Instruments, according to ASTM D2240.

3. Results and discussion

3.1. Characterization of cellulose nanocrystals

From the analysis of TEM pictures of CNC suspensions (see Fig. 1) it was possible to assess that the nanocellulose rod-like particles were roughly 400–600 nm long and 5–10 nm wide. The average ratio of length to diameter (i.e. aspect ratio, L/D) of produced CNC is around 50. The aspect ratio L/D, is a good parameter to estimate the reinforcing capacity of CNCs. Generally speaking, particles having an elevated aspect ratio exhibit a higher reinforcing capability [33]. The average L/D obtained by CNCs is in line with literature evidencing that the cellulose nanocrystals isolated from wood and cotton

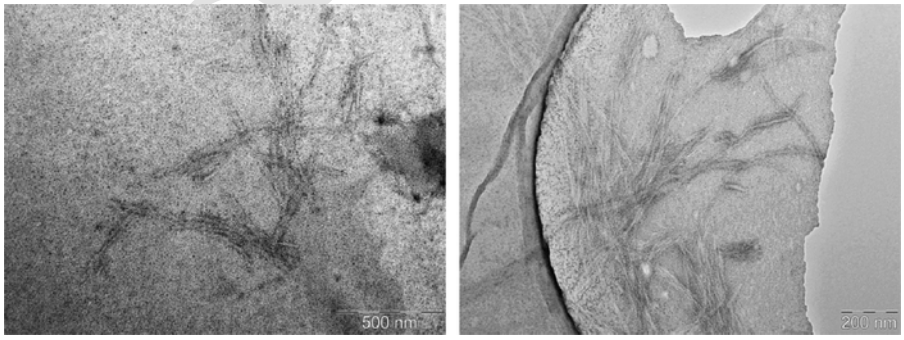

Fig. 1. TEM images of CNC particles isolated from CMC by acid hydrolysis.

sources through sulfuric hydrolysis have a L/D value between 20 and 100 [34,35].

3.2. Characterization of composites

3.2.1. Rheological behavior

The viscosity of unfilled photocurable matrix is plotted as a function of the shear rate in Fig. 2. In the same figure, the flow curves of the photomatrix filled with 5 wt% and 10 wt% of CNC particles are also displayed. The rheological curves ~~shown~~ in Fig. 2 show a pseudo-plastic behavior, evidencing the typical behavior of filled resins, i.e. the viscosity increases with increasing the weight fraction of CNC, assuming a value almost independent from the shear rate at higher values. It is worthwhile to underline that the viscosity of the innovative coatings remains suitable for the specific application even at the highest CNC content and always lower than that measured for CMC composites with the same composition [23].

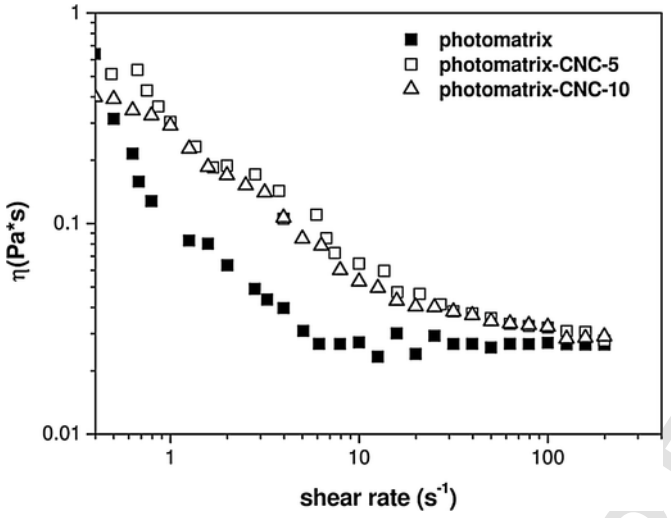

Fig. 2. Apparent viscosity of neat photomatrix and its corresponding nanocomposites.

3.2.2. Microstructure analysis

The dispersion degree of freeze-dried CNCs within the photomatrix was estimated by FESEM observations. In Fig. 3 FESEM micrographs of cryofractured surfaces of all formulations are reported. Fig. 3b and c refer to samples with 5 wt% of CNC, while Fig. 3d and e refer to samples filled with 10 wt% of CNC at different magnifications.

Reaching a high-level dispersion of hydrophilic CNCs within hydrophobic matrices is not easy because of the presence of hydrogen ~~bondings~~ among the nanocrystals that rises the agglomeration phenomena in non-polar matrices [36]. Analysing the FESEM images of filled formulation at different magnifications, it is difficult to assess the dispersion degree of CNC into the photomatrix. There is the presence of some particular structures in all filled samples. However, it is not possible to affirm if those are aggregates of CNC since a good contrast was not achieved, because CNC are transparent to electron [37].The size of these evidences seems to be around 20–40 μm, but they could be related to the creation of artifacts during the ~~breakage~~ or maybe to the increase of the surface roughness of the neat matrix.

Lewandowska and Eichhorn [36] found a similar microstructure ~~situation~~ using freeze-dried CNC into high-density polyethylene. In their work, thanks to Raman imaging and the image analysis it was possible to quantify the dispersion degree of cellulose nanocrystals within the matrix. Interestingly, starting from structures about 40 μm long, they were able to assess effective agglomeration area of few micrometers [36]. No aggregation phenomena were detected ~~for~~ microcomposites even at highest amounts of CMC. The FESEM images of CMC filled composites are reported in a previous work [23].

3.2.3. Thermal properties

The glass transition temperature (T_g) and the residual heat of curing ($\Delta H_{residual}$) values of neat photomatrix and CNC and CMC composites obtained from DSC thermograms are listed in Table 1. CNC promotes an increment of T_g of about 7 °C at the highest filler loading, while CMC does not have a comparable effect. In Fig. 4 the effects of both CMC and CNC on the relative increment of Tg of cured systems with respect to the unfilled matrix can be easily compared. It is worthwhile to note that an increase of T_g corresponds to a reduction of the mobility of polymeric chains CNC. Concurrently, both CNC and CMC filler contents higher than 5 wt% lead to an increase of the $\Delta H_{residual}$ of the photoresin. This suggests a decrease of the photocurable resin reactivity due to the light scattering of particles. Parti-

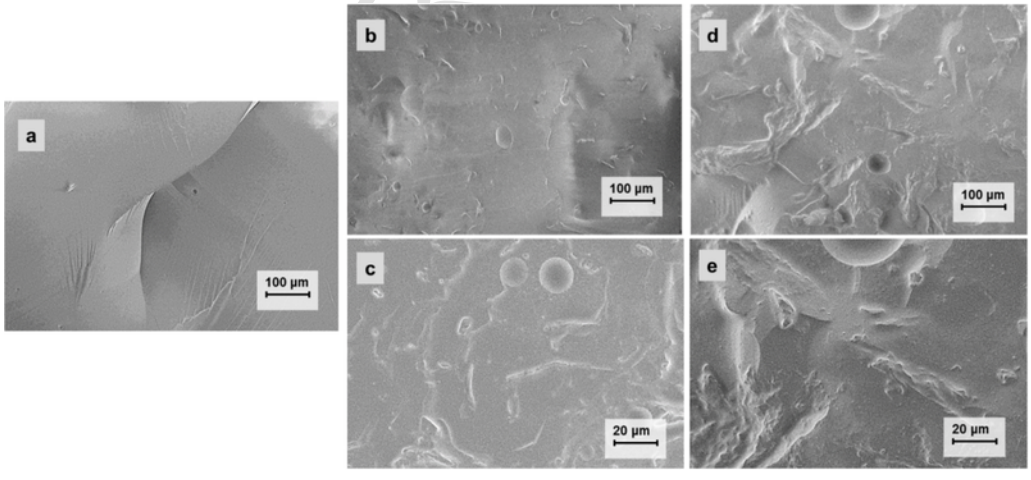

Fig. 3. FESEM images the cryofractured surfaces of (a) neat photomatrix, (b–c) photomatrix-CNC-5 at different magnification, (d–e) photomatrix-CNC-10 at different magnification.

Table 1
DSC results of neat photomatrix and corresponding nano- and microcomposites. $\Delta H_{residual}$ is the residual specific power of the cure reaction normalized to the resin content.

Sample	Tg (°C)	$\Delta H_{residual}$ (W g^{-1})
photomatrix	47.3 ± 1.1	45.8
photomatrix-CNC-5	50.8 ± 0.7	45.2
photomatrix-CNC-10	54.4 ± 1.2	56.4
photomatrix-CMC-5	48.6 ± 1.4	53.3
photomatrix-CMC-10	47.5 ± 0.9	57.8

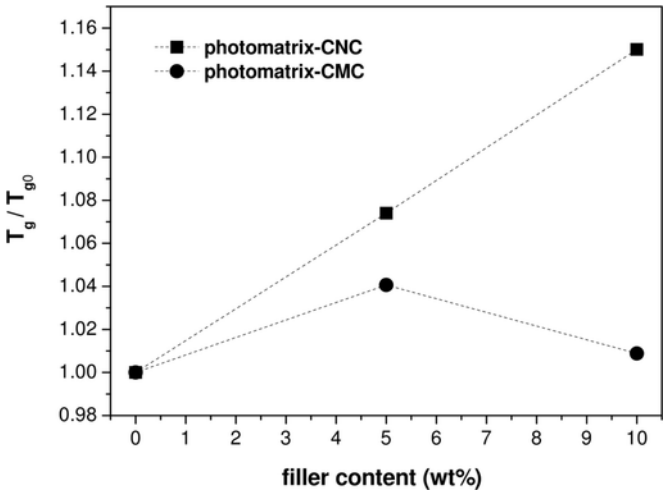

Fig. 4. Relative values of glass transition temperature of CNC and CMC filled composites.

cles may act as a shield in preventing the light penetration into the liquid system [38]. Nevertheless the reactivity of filled suspensions is still suitable for the ~~definite~~ application [39].

TGA thermograms of neat photomatrix, freeze-dried CNC and filled nanocomposites are reported in Fig. 5a, while in Fig. 5b the derivative of the mass loss curves is represented. Thermal resistance properties of the constituents and the relative CNC and CMC composites are listed in Table 2. Although the degradation of CNC occurs much earlier than that of the neat photomatrix, all filled formulations show the shift of the main degradation peak to higher temperatures (around 5 °C). Also the temperature associated to the initial degradation step, T_{onset}, increases of about 12 °C after the CNC addition of 5 wt%, while samples with 10 wt% of CNC ~~report~~ the same T_{onset} value of the neat matrix.

Comparing the results of nano- and microcomposites one can conclude that CMCs is ineffective or even detrimental on the thermal behavior of the neat matrix. Actually, if the introduction of CNC leads to an enhancement of the T_{onset}, CMC composites manifest a decrease of this temperature of about 20 °C regardless the filler loading (Table 2). The presence of cellulose compounds, regardless the particles size, lead to the formation of a solid residual. In fact, the residual mass determined at the end of the heating treatment increases proportionally to the filler content with nano- and microcomposites exhibiting a similar residual content.

3.2.4. Dynamic mechanical thermal analysis and thermal expansion coefficient

The thermograms of storage and loss moduli of neat photoresin and corresponding CNC and CMC filled composites are reported in Fig. 6, while some viscoelastic parameters of the unfilled and filled UV-light cured systems are summarized in Table 3 along with the co-

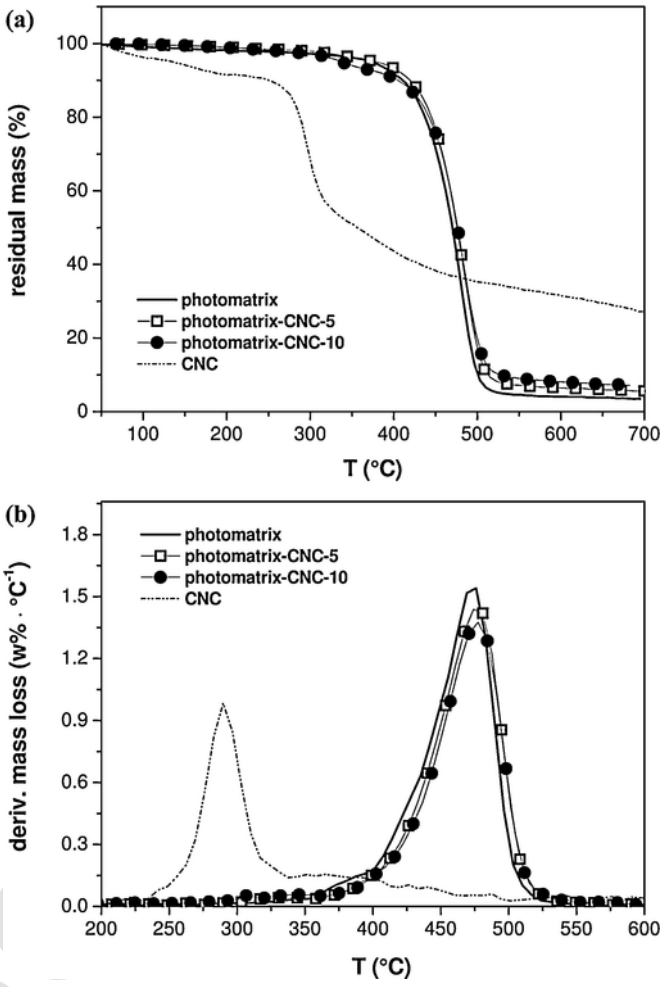

Fig. 5. TGA thermograms of neat photoresin, neat CNC, and corresponding nanocomposites. (a) Residual mass as a function of temperature, (b) derivative of the mass loss.

Table 2
Results of TGA test on neat photomatrix and corresponding nano- and microcomposites. T_{onset} is the temperature of the initial degradation step (corresponding to a mass loss of 10 wt%), while T_{MAX} is the temperature of the maximum degradation rate.

Sample	T_{onset} (°C)	T_{MAX} (°C)	Residual mass at 700 °C (%)
photomatrix	400 ± 2.0	472 ± 0.9	3.6
photomatrix-CNC-5	412 ± 1.9	477 ± 1.2	4.4
photomatrix-CNC-10	400 ± 2.1	477 ± 1.9	6.9
photomatrix-CMC-5	380 ± 0.9	472 ± 1.5	4.0
photomatrix-CMC-10	380 ± 1.7	472 ± 1.8	6.6
CNC	228 ± 1.5	290 ± 1.6	25.7
CMC	306 ± 1.9	337 ± 1.7	0.8

efficient of linear thermal expansion (CLTE) values. Nano and microcellulose produce a similar stabilizing effect on the photomatrix with a progressive enhancement of dynamic moduli (E′ and E″) and a systematic reduction of the thermal strain as the filler content increases. A remarkable effect of CNC on these parameters is evidenced from the obtained DMTA results. In Fig. 7 the comparison between CNC and CMC photocomposites viscoelastic responses is represented by the relative trends of storage modulus (E′ at 25 °C), loss modulus (E″ peak value) and coefficient of linear thermal expansion (i.e the ratios between the composites values and the neat matrix values).

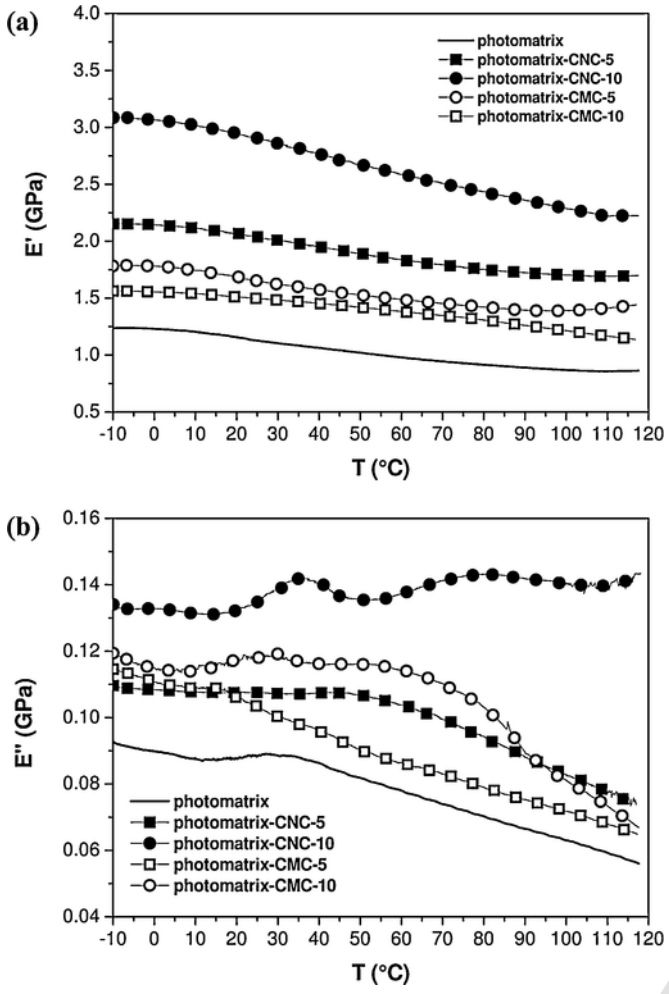

Fig. 6. DMTA thermograms of neat photoresin and corresponding CNC and CMC filled composites: (a) storage modulus E', (b) loss modulus E".

Table 3
Storage modulus (E'), loss modulus (E"), loss tangent (tanδ), glass transition temperature (Tg) and coefficient of linear thermal expansion (CLTE) values as measured by DMTA tests of neat photoresin and corresponding nano- and microcomposites.

Sample	E' (GPa) at 25 °C	E" (GPa) peak value	tanδ peak value	CLTE (10^{-6} K^{-1})
Photomatrix	1.13 ± 0.12	0.093 ± 0.012	0.074 ± 0.008	108.70 ± 0.05
photomatrix-CNC-5	2.04 ± 0.15	0.107 ± 0.003	0.064 ± 0.003	46.53 ± 0.03
photomatrix-CNC-10	2.92 ± 0.20	0.142 ± 0.008	0.055 ± 0.004	34.8 ± 0.02
photomatrix-CMC-5	1.50 ± 0.14	0.108 ± 0.003	0.069 ± 0.005	75.46 ± 0.02
photomatrix-CMC-10	1.65 ± 0.11	0.119 ± 0.008	0.053 ± 0.005	71.82 ± 0.04

Nanocomposites manifest an increment of storage and loss moduli up to 160% and 50% respectively, while microcomposites show a maximum increase of E′ and E″ until 45% and 30% respectively, in comparison to that of the neat matrix (Fig. 7a and b). For all filled formulations the increase of stiffness corresponds to a decrease of the loss factor proportionally to the filler content (Table 3). CLTE values are reduced by the presence of both cellulosic fillers. Nevertheless, CNC appears to be much more efficient than CMC in limiting the thermal

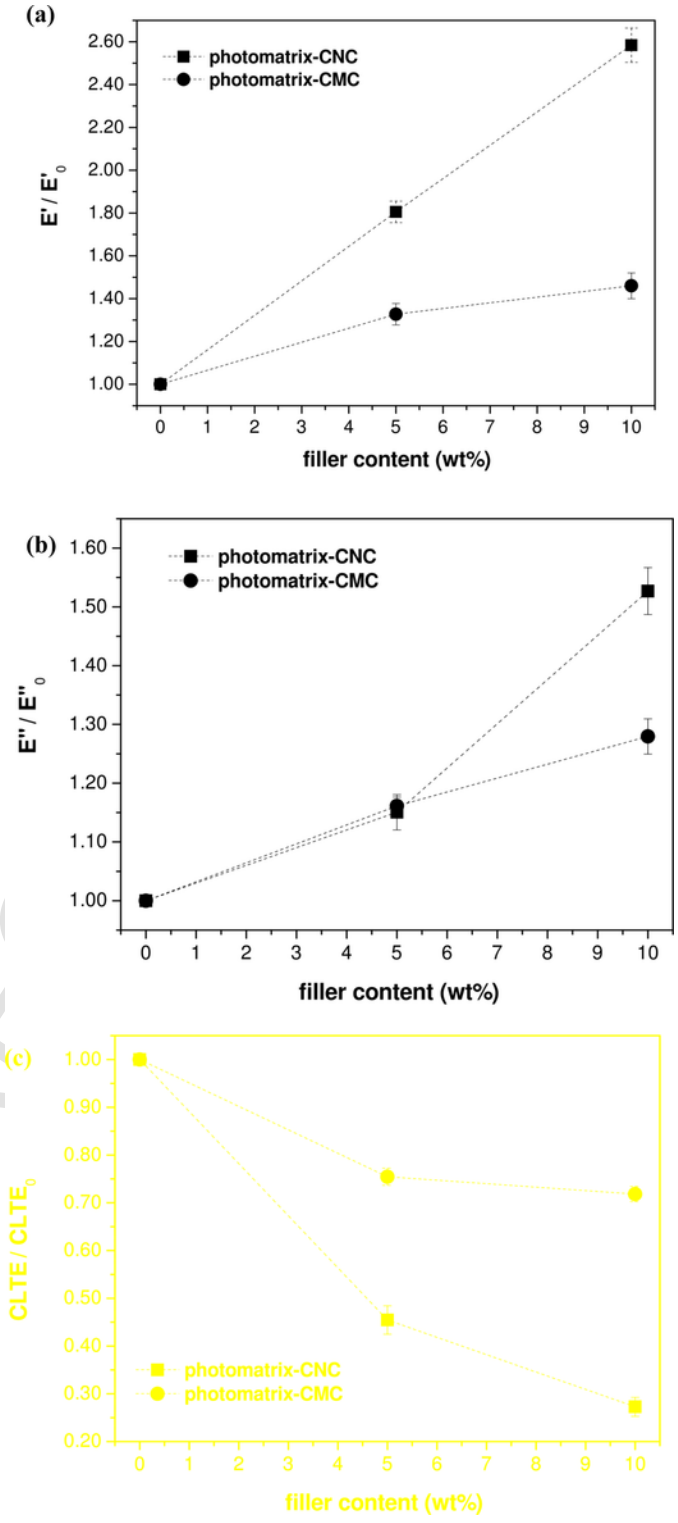

Fig. 7. Comparison between CNC and CMC filled composites response as determined from DMTA analysis at 25 °C: (a) relative storage modulus, (b) relative loss modulus, (c) relative coefficient of linear thermal expansion.

expansion of the polymer matrix reaching CLTE values about 70% lower than the neat matrix in comparison to the 25% reduction observed for ~~microcomposites~~ at the highest filler loading (Fig. 7c).

3.2.5. Mechanical properties

Fig. 8 shows the representative stress/strain curves of the neat photoresin and of the corresponding nanocomposites. Three-point bending tests confirm the stiffening effect of CNC on the photoresin due to introduction without any significant embrittling effect. In Table 4 the most important mechanical parameters measured under 3-points bending configuration are summarized for both neat photoresin and CNC or CMC filled composites. An increment of the flexural elastic modulus (E_f), a slight increase of the maximum flexural stress ($\sigma_{MAX,f}$) and a decrease of the maximum flexural strain ($\varepsilon_{MAX,f}$) with the filler loading can be observed. Even in this case it is possible to note that CNC exhibits a stronger influence on the mechanical behavior of photoresin with respect to CMC. The trend of relative modulus (i.e. E_f normalized over the corresponding value of the neat matrix) is reported in Fig. 9 for both CMC and CNC: The introduction of 10 wt% of CNC promotes an increment up to around 100% of the modulus while CMC filled composites reach a maximum increment of 50%. Similar results were found by Cataldi et al. [40] comparing the thermo-mechanical effect of nano- and microcellulose within a water soluble polymeric matrix, with a more effective action of the nanoscale filler with respect to the microscale one.

Higher aspect ratio, efficient load-carrying capabilities and mechanical properties of CNC with respect to CMC lead to a better efficiency of these nanocrystals in the improvement of the thermo-mechanical response of the neat photoresin [40].

3.2.6. Contact angle, ShoreD and pencil hardness

Hydrophobicity, surface Shore D and pencil hardness of both products were also obtained and listed in Table 5. Each system shows

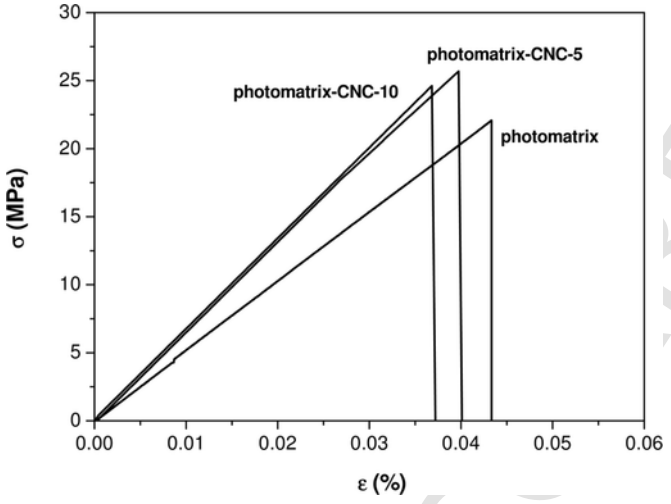

Fig. 8. Representative load/displacement curves of neat photomatrix and corresponding nanocomposites from three-points bending tests.

Table 4
Flexural modulus (E_f), maximum flexural stress ($\sigma_{MAX,f}$) and maximum flexural strain ($\varepsilon_{MAX,f}$) as measured in 3-points bending tests on neat photoresin and corresponding microcomposites.

Sample	E_f (GPa)	$\sigma_{MAX,f}$ (MPa)	$\varepsilon_{MAX,f}$
photomatrix	1.49 ± 0.04	22.19 ± 1.85	0.052 ± 0.002
photomatrix-CNC-5	2.36 ± 0.02	25.82 ± 0.34	0.041 ± 0.001
photomatrix-CNC-10	3.02 ± 0.06	23.60 ± 0.53	0.040 ± 0.001
photomatrix-CMC-5	1.98 ± 0.05	24.08 ± 1.18	0.046 ± 0.003
photomatrix-CMC-10	2.32 ± 0.05	26.75 ± 1.74	0.042 ± 0.001

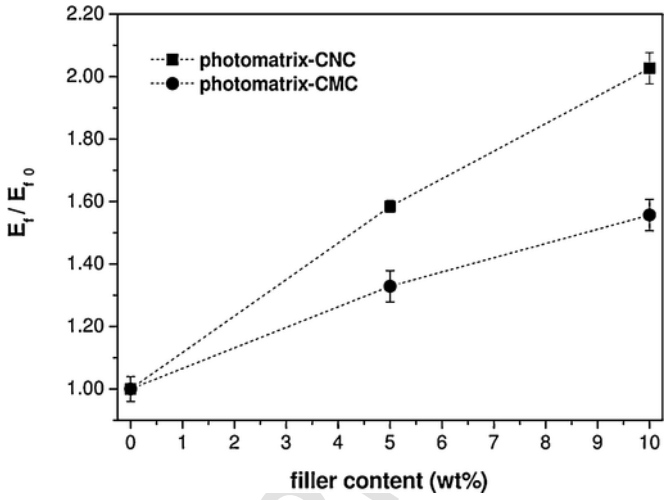

Fig. 9. Relative flexural modulus of neat photomatrix and CNC and CMC filled composites.

Table 5
Contact angle values and ShoreD and pencil hardness values of neat photoresin and corresponding microcomposites.

Sample	Contact angle (°)	ShoreD Hardness	Pencil hardness
photomatrix	103.5 ± 0.8	81.0 ± 1.6	6H
photomatrix-CNC-5	107.3 ± 0.4	92.4 ± 0.6	9H
photomatrix-CNC-10	111.1 ± 0.7	98.7 ± 0.5	9H
photomatrix-CMC-5	107.7 ± 0.7	87.1 ± 0.2	9H
photomatrix-CMC-10	107.7 ± 0.8	92.9 ± 0.3	7H

an hydrophobic behavior, evidenced by a contact angle higher than 90°, reported in Table 5. The highest contact angle of about 111°. (i.e. the strongest hydrophobic behaviour) can be observed for the sample containing the highest amount of CNC. On the other hand, Shore D surface and pencil hardness values measured on photocured- nano- and microcomposites underline that the presence of a slight amount of CNC particles (i.e. 5–10% by weight) produces the highest enhancement of the surface hardness of the neat matrix with respect to CMC filled composites. A comparable tendency in physical properties was recorded in the case ~~the~~ boehmite filled nanocomposite UV-cure coatings, as previously reported [22].

3.3. Coatings on wood

In order to assess the effect of CNC and CMC based coatings on the performances of the neat photomatrix as protective coating on wood, unfilled and filled formulations were applied on walnut wood samples as depicted in Fig. 10. The results, reported in Table 6 for walnut wood treated with both unfilled and CNC or CMC filled coatings, prove that each system was able to improve the physical properties of wood, in terms of water sorption, hydrophobicity and surface hardness. Even in this case, samples protected with the nanofilled coatings show the best performances. As far as the contact angle values is concerned, all walnut wood samples treated with the photo-polymerizable coatings exhibit a value higher than 100°. Interestingly, ~~those~~ samples treated with the nanofilled coatings reach the highest contact angle, i.e. about 130°, comparable to the values registered for ~~the best~~ commercial protective products for wood [30]. While the presence of CMC does not produce any relevant effect on the hydrophobic features of the neat matrix.

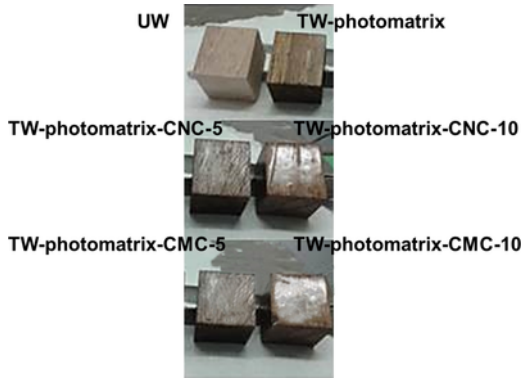

Fig. 10. Images of walnut wood samples treated with unfilled (TW-photomatrix) and CNC filled formulations (TW-photomatrix-CNC) and CMC filled composites (TW-photomatrix-CMC).

Table 6
Water absorption percentage, Color change evaluation results, Contact angle values and ShoreD and pencil hardness values of walnut wood samples untreated (UW) and treated with neat photomatrix (TW-photomatrix) and its CNC and CMC composites (TW-photomatrix-CNC and TW-photomatrix-CMC, respectively).

Sample	WA_t (%)	Sorptivity coefficient (g/cm^{2}s$^{1/2}$)	Color variation ΔE	Contact angle (°)	ShoreD Hardness
UW	144.88	1.91	–	56.35 ± 4.1	61.03 ± 6.45
TW-photomatrix	87.34	0.90	9.15	106.3 ± 1.1	65.03 ± 1.25
TW-photomatrix-CNC-5	50.31	0.0084	10.58	132.1 ± 0.9	69.44 ± 3.21
TW-photomatrix-CNC-10	13.00	0.0080	10.08	131.3 ± 0.6	71.13 ± 2.47
TW-photomatrix-CMC-5	72.89	0.66	12.89	109.45 ± 1.1	68.24 ± 2.7
TW-photomatrix-CMC-10	75.40	0.36	13.01	108.22 ± 0.9	66.22 ± 3.1

WAt: water absorption values.
ΔE: color variation.

Since in porous building materials, such as wood, concrete, brick, mortar and stone, water sorptivity (i.e., water capillary absorption rate) which describes the amount of water that penetrates into the material per unit surface area per square root of time is a key parameter, the water absorption kinetics of both coated and uncoated specimens of walnut wood, were finally determined by using the procedure previous described [41]. The experimental results obtained are shown in Fig. 11. Each point of the kinetics curves represents the average weight measurements of a set of ten specimens per sample. The water sorptivity of the wood was, hence, determined according to European Standard 15801 ("European standard 15801, Conservation of cultural property − test methods − determination of water absorption by capillarity, 2010," 2010), starting from data reported in Fig. 11. In details, during capillary absorption, the sorptivity coefficient was calculated as the slope of the linear part of the graph obtained by plotting the weight increase for unit surface vs. the square root of time, hence its value corresponds to a constant rate of change of the phenomenon. As expected, the water absorption capacity of the coated samples was greatly reduced with respect to uncoated specimens, in particular in the case of the wood coated with the formulation with the highest loaded of CNC. In details, the samples coated with nanocomposites

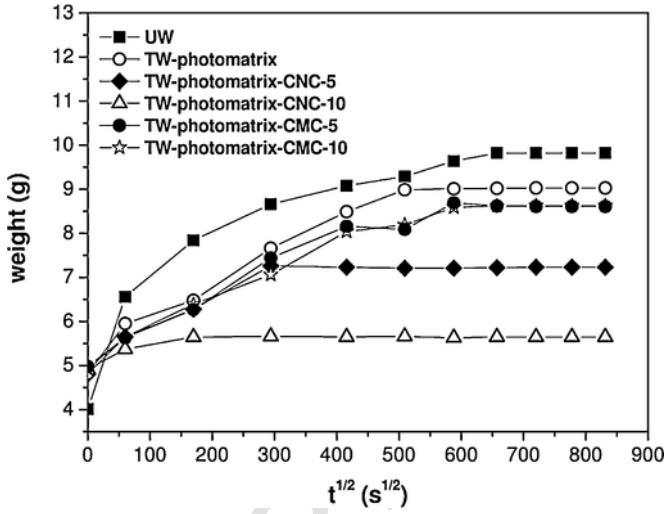

Fig. 11. Representative capillary water sorption curves of walnut wood samples untreated and treated with unfilled and nano and microstructured photo-curable composites.

absorb much less water not only respect to the uncoated wood, but also respect to wood coated with unfilled coating. This different behaviour was quantified by determining the final water absorption values (WAt), calculated according to Eq. (1) and the sorpitivity coefficient for treated and control wood specimens. and reported in Table 6. One can notice the outstanding hydrophobic capability of the nanofilled coatings containing 10 wt% of CNC that report a WAt value of 13% with respect to the neat matrix and especially to CMC filled composites showing a final WAt value of 87% and 73–75%, respectively.

All wood treated samples exhibit a higher value of surface hardness. The increment of this property is remarkable for samples coated with CNC filled composites. In Fig. 12 it is possible to evaluate the state of treated wood samples after the water sorption test. Interestingly, samples treated with CNC filled formulations show the best appearance and the absence of relevant damage, while the samples coated with the neat photomatrix and especially with microcomposites exhibit the worst conditions.

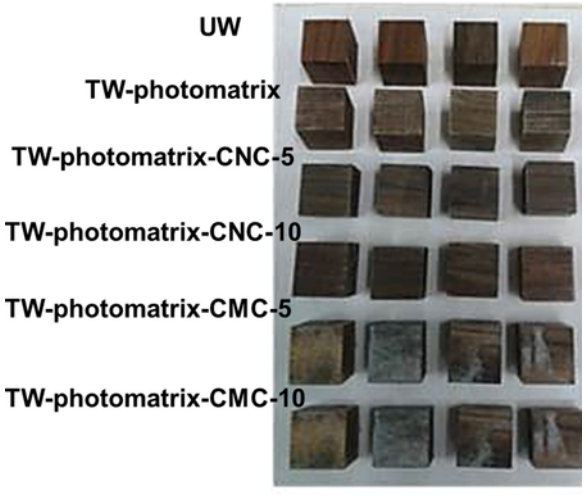

Fig. 12. Images of walnut wood samples treated with unfilled (TW-photomatrix) and CNC filled formulations (TW-photomatrix-CNC) and CMC filled composites (TW-photomatrix-CMC) after water sorption test.

Finally the color change of the treated wood samples was also estimated and the results are reported in Table 6. The presence of the treatment, in particular, in the case of the filled coatings causes an alteration of the natural color of the wood sample (Fig. 12), even if to a limited extent, since a ΔE less than 11 was determined for nanocomposites [8]. CMC filled formulations lead to the highest chromatic variation (about 13) of the wood after treatment.

4. Conclusions

Both cellulose nanocrystals and microcrystals were dispersed in a UV-light-photocurable methacrylic-siloxane resin in order to estimate their effect on the properties of the resin and to assess their suitability to be used as protective coatings on wood. Only CNC was able to effectively increase the thermal properties of the neat matrix. Nanocellulose promoted the best increment of the stiffness into the neat cured systems in comparison to microcellulose response. No embrittling of the matrix was observed after the introduction of both CNC and CMC. A more pronounced enhancement of the hydrophobicity (contact angle), surface hardness (Shore D and pencil scratch tests) of the neat matrix filled with CNC was detected. Interestingly, application of CNC-filled coatings on wood confirmed their higher efficiency with respect to CMC-filled coatings in reducing the water sorption of wood through a modification of the hydrophobicity and surface hardness of wood.

Acknowledgments

Mrs. Gloria Ischia for her support the TEM observations, Mr. Lorenzo Moschini for his assistance with FESEM analysis and the Biotech Lab for allowing the freeze-drier use are kindly acknowledged.

References

[1] A. Cataldi, F. Deflorian, A. Pegoretti, Microcrystalline cellulose filled composites for wooden artwork consolidation: application and physic-mechanical characterization, Mater. Des. 83 (2015) 611–619.
[2] V. Horie, Materials for Conservation: Organic Consolidants, Adhesives and Coatings, Routledge, 2010.
[3] L. Bertolini, Materiali da costruzione. Degrado, prevenzione, diagnosi, restauro, Città Studi Edizioni (2006).
[4] L. Toniolo, A. Paradisi, S. Goidanich, G. Pennati, Mechanical behaviour of lime based mortars after surface consolidation, Constr. Build. Mater. 25 (2011) 1553–1559.
[5] G. Borsoi, M. Tavares, R.V. António Santos Silva, Studies of the Performance of Nanostructured and other Compatible Consolidation Products for Historical Renders, in: Mater. Sci. Forum, Ana Maria Pires Pinto and António Sérgio Pouzada (2012), pp. 942–947.
[6] C.A.S. Hill, Impregnation modification, Wood Modification, John Wiley & Sons Ltd, 2006149–173.
[7] W.J. Homan, A.J.M. Jorissen, Wood modification developments, Heron 49 (2004) 361–385.
[8] B.C. Kielmann, C. Mai, Application and artificial weathering performance of translucent coatings on resin-treated and dye-stained beech-wood, Prog. Org. Coat. 95 (2016) 54–63.
[9] M. Robson, Early advances in the use of acrylic resins for the conservation of antiquities, in: N.S. Allen, M. Edge, C.V. Horie (Eds.), Polymers in Conservation, Royal Society of Chemistry, Cambridge U.K, 1992, p. 184.
[10] E.F. Hansen, R. Lowinger, E. Sadoff, Consolidation of porous paint in a vapor-saturated atmosphere, J. Am. Inst. Conserv. 32 (1993) 0–14.
[11] C. Miliani, M. Ombelli, A. Morresi, A. Romani, Spectroscopic study of acrylic resins in solid matrices, Surf. Coat. Technol. 151–152 (2002) 276–280.
[12] G.G. Amoroso, M. Camaiti, Trattato di scienza della conservazione dei monumenti: etica della conservazione, degrado dei monumenti, interventi conservativi, consolidanti e protettivi, Alinea (2002).
[13] A. Kaboorani, N. Auclair, B. Riedl, V. Landry, Physical and morphological properties of UV-cured cellulose nanocrystal (CNC) based nanocomposite coatings for wood furniture, Prog. Org. Coat. 93 (2016) 17–22.
[14] F. Grüneberger, T. Künniger, A. Huch, T. Zimmermann, M. Arnold, Nanofibrillated cellulose in wood coatings: dispersion and stabilization of ZnO as UV absorber, Prog. Org. Coat. 87 (2015) 112–121.
[15] F. Girardi, E. Cappelletto, J. Sandak, G. Bochicchio, B. Tessadri, S. Palanti, E. Feci, R. Di Maggio, Hybrid organic–inorganic materials as coatings for protecting wood, Prog. Org. Coat. 77 (2014) 449–457.
[16] F.Z. Feng, F.J. N., L.H. S., Wood coating and coating technology, Chemical Industry Press Beijing (2008).
[17] K.D. Weiss, Paint and coatings: a mature industry in transition, Prog. Polym. Sci. 22 (1997) 203–245.
[18] P.J.A. Geurink, T. Scherer, R. Buter, A. Steenbergen, H. Henderiks, A complete new design for waterborne 2-pack PUR coatings with robust application properties, Prog. Org. Coat. 55 (2006) 119–127.
[19] R.L. Clough, High-energy radiation and polymers: a review of commercial processes and emerging applications, Nucl. Instrum. Methods Phys. Res. Sect. B: Beam Interact. Mater. Atoms 185 (2001) 8–33.
[20] R. Schwalm, U.V. Coatings, UV Coatings: Basics, Recent Developments and New Applications, Elsevier Science, 2006.
[21] C. Decker, The use of UV irradiation in polymerization, Polym. Int. 45 (1998) 133–141.
[22] C. Esposito Corcione, R. Manno, M. Frigione, Sunlight curable boehmite/siloxane-modified methacrylic nano-composites: an innovative solution for the protection of carbonate stones, Prog. Org. Coat. 97 (2016) 222–232.
[23] A. Cataldi, C. Esposito Corcione, M. Frigione, A. Pegoretti, Photocurable resin/microcrystalline cellulose composites for wood protection: physical-mechanical characterization, Prog. Org. Coat. 99 (2016) 230–239.
[24] J.F. Revol, H. Bradford, J. Giasson, R.H. Marchessault, D.G. Gray, Helicoidal self-ordering of cellulose microfibrils in aqueous suspension, Int. J. Biol. Macromol. 14 (1992) 170–172.
[25] W. Bai, J. Holbery, K. Li, A technique for production of nanocrystalline cellulose with a narrow size distribution, Cellulose 16 (2009) 455–465.
[26] J.P.F. Lagerwall, C. Schutz, M. Salajkova, J. Noh, J. Hyun Park, G. Scalia, L. Bergstrom, Cellulose nanocrystal-based materials: from liquid crystal self-assembly and glass formation to multifunctional thin films, NPG Asia Mater. 6 (2014) e80.
[27] K.-Y. Lee, Y. Aitomäki, L.A. Berglund, K. Oksman, A. Bismarck, On the use of nanocellulose as reinforcement in polymer matrix composites, Compos. Sci. Technol. 105 (2014) 15–27.
[28] N. Lavoine, I. Desloges, A. Dufresne, J. Bras, Microfibrillated cellulose—its barrier properties and applications in cellulosic materials: a review, Carbohydr. Polym. 90 (2012) 735–764.
[29] A. Dufresne, Nanocellulose: a new ageless bionanomaterial, Mater. Today 16 (2013) 220–227.
[30] C. Esposito, M. Frigione, Novel UV-cured nanocomposites used for the protection of walnut wood artworks, Wood Res. 59 (2014) 229–244.
[31] D. Bondeson, A. Mathew, K. Oksman, Optimization of the isolation of nanocrystals from microcrystalline celluloseby acid hydrolysis, Cellulose 13 (2006) 171–180.
[32] E.D. Cranston, D.G. Gray, Morphological and optical characterization of polyelectrolyte multilayers incorporating nanocrystalline cellulose, Biomacromolecules 7 (2006) 2522–2530.
[33] J. George, S.N. Sabapathi, Cellulose nanocrystals: synthesis, functional properties, and applications, Nanotechnol. Sci. Appl. 8 (2015) 45–54.
[34] S. Beck-Candanedo, M. Roman, D.G. Gray, Effect of reaction conditions on the properties and behavior of wood cellulose nanocrystal suspensions, Biomacromolecules 6 (2005) 1048–1054.
[35] B.L. Peng, N. Dhar, H.L. Liu, K.C. Tam, Chemistry and applications of nanocrystalline cellulose and its derivatives: a nanotechnology perspective, Can. J. Chem. Eng. 89 (2011) 1191–1206.
[36] A.E. Lewandowska, S.J. Eichhorn, Quantification of the degree of mixing of cellulose nanocrystals in thermoplastics using Raman spectroscopy, J. Raman Spectrosc. (2016). n/a-n/a.
[37] V. Vardanyan, B. Poaty, V. Landry, G. Chauve, T. Galstian, B. Riedl, 8–wear resistance of nanocomposite coatings A2–aliofkhazraei, mahmood, Anti-Abrasive Nanocoatings, Woodhead Publishing, 2015201–223.
[38] A. Licciulli, C. Esposito Corcione, A. Greco, V. Amicarelli, A. Maffezzoli, Laser stereolithography of ZrO2 toughened Al2O3, J. Eur. Ceram. Soc. 25 (2005) 1581–1589.
[39] C.E. Corcione, M. Frigione, UV-cured polymer-boehmite nanocomposite as protective coating for wood elements, Prog. Org. Coat. 74 (2012) 781–787.
[40] A. Cataldi, L. Berglund, F. Deflorian, A. Pegoretti, A comparison between micro- and nanocellulose-filled composite adhesives for oil paintings restoration, Nanocomposites 1 (2015) 195–203.
[41] G. Pia, E. Sassoni, E. Franzoni, U. Sanna, Predicting capillary absorption of porous stones by a procedure based on an intermingled fractal units model, Int. J. Eng. Sci. 82 (2014) 196–204.